A MESH-FREE NUMERICAL METHOD
FOR THE ESTIMATION OF THE TORSIONAL STIFFNESS OF LONG BONES

Anita Uscilowska and Agnieszka Fraska

A MESH-FREE NUMERICAL METHOD
FOR THE ESTIMATION OF THE TORSIONAL STIFFNESS OF LONG BONES

ANITA USCILOWSKA AND AGNIESZKA FRASKA

This paper considers the torsional stiffness of long bones. The phenomenon of long-bone twisting is a boundary value problem. We propose to solve the problem by a numerical procedure based on a mesh-free method, the method of fundamental solutions.

1. Introduction

External loads acting on long bones can cause fractures. A fracture is any break in a bone or cartilage. It usually is a result of trauma but can be due to an acquired disease of the bone such as osteoporosis or abnormal formation of the bone due to a congenital disease of the bone such as osteogenesis imperfecta. Fractures are classified by their character and location. Examples of classifications include "spiral fracture of the femur," "greenstick fracture of the radius," "impacted fracture of the humerus," "linear fracture of the ulna," "oblique fracture of the metatarsal," "compression fracture of the vertebrae," and "depressed fracture of the skull." A "comminuted fracture" is a fracture in which the bone is broken into a number of pieces, as distinguished from a "compound fracture" in which the bone sticks through the skin. The problem addressed in this paper is the twisting of a lone bone, which can cause spiral fracture of a long bone (Figure 1).

Figure 1. Spiral fracture [Pierce et al. 2004].

There are some papers in the literature treating problem of the torsional stiffness of a long bone. Comparative studies of long-bone biomechanics in primates frequently use the polar moment of inertia as a variable reflecting overall mechanical rigidity, average bending rigidity, or resistance to torsional shear stresses. Daegling [2002] showed that while the use of this variable for characterizing the first two properties is appropriate, it is potentially a highly misleading measure of torsional resistance. Indeed, theoretical and experimental research has shown that the use of the polar moment of inertia for estimating long-bone torsional rigidity should be restricted to samples of relatively invariant or cylindrical geometry.

The open section effect in a long bone with a longitudinal defect is the subject of [Elias et al. 2000], where it was found that a longitudinal defect dramatically alters the stress distribution within a long bone. For applied torsion, the defect interrupts the normal shear flow around the bone. The problem is solved by the finite element method (FEM).

Bone material properties. Bone in a living animal consists of both living tissue and nonliving substances. Within live bone are blood vessels, nerves, collagen, and living cells, including osteoblasts (cells that help form bone), and osteoclasts (cells that help eat away old bone). In addition, bone contains cells called osteocytes, which are mature osteoblasts that have ended their bone-forming careers. The nonliving, but very important, substances in bone are minerals and salts. Besides the metabolically active cellular portion of bone tissue, bone is also made up of a matrix (a bonding of multiple fibers and chemicals) of different materials, including primarily collagen fibers and crystalline salts. The crystalline salts deposited in the matrix of bone are composed principally of calcium and phosphate, which are combined to form hydroxyapatite crystals. In particular, it is the collagen fibers and calcium salts that help to strengthen bone. In fact, the collagen fibers of bone have great tensile strength (the strength to endure stretching forces), while the calcium salts, which are similar in physical properties to marble, have great compressional strength (the strength to endure squeezing forces). These combined properties, plus the degree of bondage between the collagen fibers and the crystals, provide a bony structure that has both extreme tensile and compressional strengths. Due to such a complicated structure the bone is treated as a object made with functionally graded material (FGM) [Pompe et al. 2003]. FGMs are materials with continuously varying material properties designed for specific engineering and bioengineering applications. Although the torsion problem for homogeneous linearly elastic bars is a classical one in elasticity, there has been relatively little attention paid to the case when material is inhomogeneous.

Recently, research activity on functionally graded materials has also stimulated investigation on the torsion problem for inhomogeneous material. Chen [1964] studied the torsion of inhomogeneous bars. He presented governing equations and boundary conditions for the torsion problem of inhomogeneous bars in terms of a stress function. Then, he applied a semiinverse method and found a specific distribution for the shear modulus of rigidity in a specific geometry of cross-section. By this method, he could find simple solutions for the stress function and torsional stiffness of circular and elliptical shafts. An analytical formulation for torsional analysis of functionally graded elastic bars with circular cross-sections was presented by Horgan and Chan [1999]. They supposed the shear modulus of rigidity to be a function of radius. Using the axisymmetric geometry of the cross-section of the circular bar, they found an exact analytical solution. They used governing equations and boundary conditions in terms of Prandtl's stress function. Saint-Venant's torsion problem for linearly elastic, isotropic, nonhomogeneous cylindrical bars was considered in [Ecsedi 2009].

The novelty of this paper is that the shear modulus of the investigated nonhomogeneous bar is a given function of the Prandtl stress function of a homogeneous bar, which has the same cross-sections as the nonhomogeneous bar considered. The main result of the present paper is a contribution to the existing exact benchmark solutions for functionally graded twisted elastic cylinders. Five examples (a hollow elliptical cylinder, a solid equilateral triangle cross-section, an approximate solution for a thin-walled tube, a rectangular cross-section, and a narrow rectangular cross-section) illustrate the application of the proposed method. In [Arghavan and Hematiyan 2009] an analytical formulation was presented for the torsion of functionally graded hollow tubes of arbitrary shape. The authors assumed that the thicknesses of all segments of the cross-section were the same and the shear modulus of rigidity changed continuously across the thickness. In this way the simple but relatively accurate formulas for the stresses and torsional stiffness were obtained on the basis of analytical integration of the governing equation for the stress function.

As this short review shows, the uniform torsion problem for functionally graded materials has been solved primarily by analytical methods and traditional mesh methods such as FEM [Arghavan and Hematiyan 2009] and FED [Ely and Zienkiewicz 1960]. The purpose of this paper is the application of the method of fundamental solutions (MFS) to the torsion problem of functionally graded materials. This method belongs to the so-called meshless methods which have become more and more popular in the two last decades. The MFS was first proposed in [Kupradze and Aleksidze 1964]. Its numerical implementation was carried out in [Mathon and Johnston 1977]. Comprehensive reviews of the MFS for various applications can be found in [Fairweather and Karageorghis 1998; Golberg and Chen 1999]. Here, based on the Saint-Venant displacement assumption, the boundary-value linear problem for the stress function is formulated. For isotropic materials the governing equation is linear with constant coefficients. The torsion problem for rods made with isotropic materials is solved by the MFS. For FGM the governing equation is a linear one with variable coefficients. The torsion problem for rods made with FGMs is solved by means of Picard iteration. The proposed algorithm is based on the solution of a linear Poisson equation at each iteration step. The mentioned boundary value problem is solved by the MFS with interpolation of the right-hand side by a radial basis function.

2. Problem description

The following assumptions about bone characteristics are made:

- Nonuniform bone geometry is analyzed as a tube with a constant cross-section (circular), neglecting lengthwise variations in bone geometry.

- The areal properties of the smallest bone section are taken into account.

- The bone material is considered as a functionally graded material (FGM) (the shear modulus is a function of geometrical variables).

The steady-state problem of the torsion of a long bone is modeled as the torsion of a bar with circular cross-section with a circular hollow. It is assumed that the bar is made of FGM, that is, the shear modulus is a function of geometric variables. The cross-section of the region of the bar under consideration is presented in Figure 2. The Oz-axis is directed parallel to the generators of the cylindrical surface. There are no normal stresses on the end cross-section. The applied tangential forces on the end cross-section
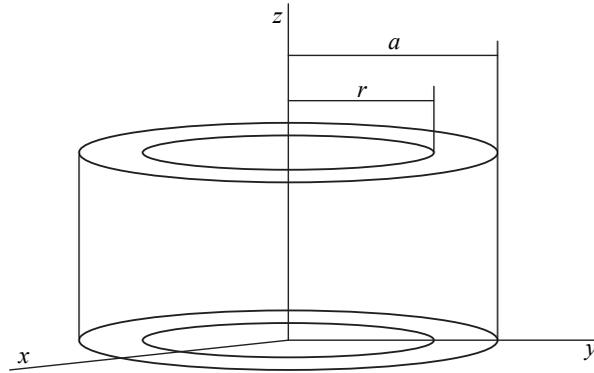
Figure 2. Geometry of the porous medium.

are equivalent to two couples whose magnitudes are the same and whose moments are directed along the
z-axis in opposite directions.

3. The equations of strength theory

To introduce the equations governing the torsion of a bar with circular cross-section, general strength
theory is applied. The geometry of the bar is presented in Figure 2. The displacement components in
cylindrical coordinates are

$$u_x(x, y, z), \ u_y(x, y, z), \ u_y(x, y, z). \tag{3-1}$$

As in homogeneous Saint-Venant theory, let us assume that all the stress components are zero except for
τ_{xz} and τ_{yz}. The assumption of strength theory allows the introduction of the Prandtl stress function ψ,
which is defined by the stresses as follows:

$$\tau_{xz} = \omega \frac{\partial \psi}{\partial y}, \quad \tau_{yz} = -\omega \frac{\partial \psi}{\partial x}, \tag{3-2}$$

where ψ is the Prandtl stress function, τ_{xz} and τ_{yz} are stress tensor components, and ω is the twist angle.
The equilibrium equation is automatically satisfied by (3-2) and the resulting compatibility equations are

$$\frac{\partial}{\partial x}\left(\frac{1}{G(x, y)}\frac{\partial \psi}{\partial x}\right) + \frac{\partial}{\partial y}\left(\frac{1}{G(x, y)}\frac{\partial \psi}{\partial y}\right) = -2\omega \quad \text{for } (x, y) \in \Omega, \tag{3-3}$$

where Ω is the area of the bar cross-section and $G(x, y)$ is a function defining the shear modulus of
the FGM which is assumed to be a continuously differentiable positive function on Ω. The boundary
conditions for the problem are described below.

The traction-free boundary condition on the lateral surface is fulfilled if

$$\psi = 0 \quad \text{for } (x, y) \in \Gamma. \tag{3-4}$$

In the case of a bar with a multiconnected cross-section we get the condition

$$\psi = \psi_0 \quad \text{for } (x, y) \in \Gamma_{\text{I}}, \tag{3-5}$$

where ψ_0 is an unknown constant on the inner contour Γ_I, which is determined from

$$\oint_{\Gamma_I} \frac{\partial \psi}{\partial n} \, ds = -\oint_{\Gamma_I} \frac{1}{f(x, y)} (x \, dy - y \, dx) - \oint_{\Gamma_I} \frac{1}{f(x, y)} \, du_z, \tag{3-6}$$

where Γ and Γ_I are respectively the outer and inner boundaries of the bar cross-section, Ω_I is the area of the hollow, and du_z is the deflection along the z-axis. The stiffness of the bar is defined by

$$S = 2 \iint_\Omega \psi(x, y) \, dx \, dy. \tag{3-7}$$

Thus the torsion problem of the inhomogeneous bar reduces to solving (3-3) on the domain Ω subjected to the boundary conditions (3-4)–(3-6). The corresponding stresses are given by (3-2).

To make numerical calculations more convenient dimensionless variables are introduced:

$$X = \frac{x}{a}, \quad Y = \frac{y}{a}, \quad E = \frac{r}{a}, \quad \Psi(x, y) = \frac{\psi(x, y)}{a^2 G_0}, \quad f(x, y) = \frac{G_0}{G(x, y)}, \tag{3-8}$$

where G_0 is constant which has dimension of the shear modulus and a is a characteristic dimension.

Considering the problem for dimensionless variables and using the symmetry of the region $\tilde{\Omega}$ presented in Figure 3 gives the equation

$$\frac{\partial}{\partial X} \left(f(X, Y) \frac{\partial \Psi}{\partial X} \right) + \frac{\partial}{\partial Y} \left(f(X, Y) \frac{\partial \Psi}{\partial Y} \right) = -2 \quad \text{for } (X, Y) \in \tilde{\Omega}. \tag{3-9}$$

The boundary conditions after introducing the dimensionless variables are:

- for the outer boundary:

$$\Psi = 0 \quad \text{for } (x, y) \in \tilde{\Gamma}; \tag{3-10}$$

- for the hollow boundary:

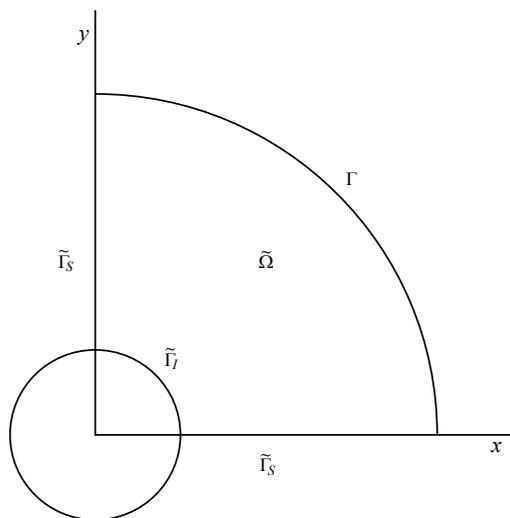$$\Psi = \Psi_0 \quad \text{for } (x, y) \in \tilde{\Gamma}_I; \tag{3-11}$$

Figure 3. The region under consideration in dimensionless form.

and

$$\oint_{\tilde{\Gamma}_I} \frac{\partial \Psi}{\partial n}\, ds = -\oint_{\tilde{\Gamma}_I} \frac{1}{f(X,Y)}(X\,dY - Y\,dX) - \oint_{\tilde{\Gamma}_I} \frac{1}{f(X,Y)}\, d\tilde{u}_z, \tag{3-12}$$

where $\tilde{\Gamma}$ is the outer boundary of the bar cross-section, $\tilde{\Gamma}_I$ is the inner boundary of the bar cross-section, $\tilde{\Omega}_I$ is the area of the hollow, and $\tilde{u}_z = u_z/a$ is the dimensionless deflection along the z-axis. The extra condition appears for the symmetry of the region considered:

$$\frac{\partial \Psi}{\partial n} = 0 \quad \text{for } (x,y) \in \tilde{\Gamma}_{\mathrm{S}}. \tag{3-13}$$

4. The numerical method for solving the boundary value problem

The proposal of this paper is to solve the boundary value problem given above by a mesh-free method, the method of fundamental solutions (MFS). The differential equation (3-9) is of the second order with variable coefficients. A procedure based on Picard iteration is proposed to solve the problem of such an equation. Equation (3-9) is rewritten in iterative fashion:

$$\frac{\partial^2 \Psi^{(i)}}{\partial X^2} + \frac{\partial^2 \Psi^{(i)}}{\partial Y^2} = -\frac{1}{f(X,Y)}\left(2 + \frac{\partial f}{\partial X}\frac{\partial \Psi^{(i-1)}}{\partial X} + \frac{\partial f}{\partial Y}\frac{\partial \Psi^{(i-1)}}{\partial Y}\right) \quad \text{for } (X,Y) \in \tilde{\Omega}, \tag{4-1}$$

for $i = 1, 2, \ldots$. The boundary conditions have the form

$$\Psi^{(i)} = 0 \quad \text{for } (X,Y) \in \tilde{\Gamma}, \tag{4-2}$$

$$\Psi^{(i)} = \Psi_0 \quad \text{for } (X,Y) \in \tilde{\Gamma}_I, \tag{4-3}$$

$$\oint_{\tilde{\Gamma}_I} \frac{\partial \Psi^{(i)}}{\partial n}\, ds = -\oint_{\tilde{\Gamma}_I} \frac{1}{f(X,Y)}(X\,dY - Y\,dX) - \oint_{\tilde{\Gamma}_I} \frac{1}{f(X,Y)}\, d\tilde{u}_z, \tag{4-4}$$

$$\frac{\partial \Psi^{(i)}}{\partial n} = 0 \quad \text{for } (X,Y) \in \tilde{\Gamma}_{\mathrm{S}}. \tag{4-5}$$

At each iteration step, the boundary value problem with the Poisson-like equation (4-1) and the boundary conditions (4-2)–(4-5) is to be solved. The governing equation is rewritten in a very general form:

$$L\Psi^{(i)}(X,X) = F\big(X, Y, \Psi^{(i-1)}(X,Y)\big) \quad \text{for } (X,Y) \in \tilde{\Gamma}_{\mathrm{S}}, \tag{4-6}$$

where L is the Laplace operator. The function on the right-hand side of the equation is

$$F\big(X, Y, \Psi^{(i-1)}(X,Y)\big) = -\frac{1}{f(X,Y)}\left(2 + \frac{\partial f}{\partial X}\frac{\partial \Psi^{(i-1)}}{\partial X} + \frac{\partial f}{\partial Y}\frac{\partial \Psi^{(i-1)}}{\partial Y}\right). \tag{4-7}$$

The boundary conditions (4-2)–(4-5) are still valid. It is assumed that the solution of the problem is a sum of particular and homogeneous solutions:

$$\Psi^{(i)}(X,Y) = \Psi_p^{(i)}(X,Y) + \Psi_h^{(i)}(X,Y). \tag{4-8}$$

The particular solution is related to the right-hand-side function of the inhomogeneous equation (4-6). The function (4-7) is interpolated by means of radial basis functions (RBFs) in the following manner:

$$F\big(X, Y, \Psi^{(i-1)}(X, Y)\big) = \sum_{k=1}^{Na} a_k^{(i)} \varphi_k(X, Y) + \sum_{l=1}^{Nl} b_l^{(i)} p_l(X, Y), \tag{4-9}$$

where $\varphi_k(X, Y) = \varphi\big(X, Y, X_k^{(a)}, Y_k^{(a)}\big)$ is a RBF, $\big\{X_k^{(a)}, Y_k^{(a)}\big\}_{k=1}^{Na}$ is the set of approximation points (see Figure 4) in the region $\tilde{\Omega}$, N_a is the number of approximation points, and $p_l(X, Y)$ for $l = 1, 2, \ldots, N_l$ are monomials. Moreover, $\{a_k^{(i)}\}_{k=1}^{Na}$ and $\{b_l^{(i)}\}_{l=1}^{Nl}$ are sets of real numbers, which are determined in each iterative step. The approximated particular solution has the form

$$\Psi^{(i)}(X, Y) = \sum_{k=1}^{Na} a_k^{(i)} \phi_k(X, Y) + \sum_{l=1}^{Nl} b_l^{(i)} P_l(X, Y), \tag{4-10}$$

where $\phi_k(X, Y)$ and $P_l(X, Y)$ functions are particular solutions of the equations

$$L\phi_k(X, X) = \varphi_k(X, X) \quad \text{for} \quad k = 1, 2, \ldots, N_a, \tag{4-11}$$

$$L P_l(X, Y) = p_l(X, Y) \quad \text{for} \quad l = 1, 2, \ldots, N_l. \tag{4-12}$$

The approximation formula at the i-th iterative step ($i = 1, 2, \ldots$) is written for every approximation point chosen in the domain

$$F\big(X_j^{(a)}, Y_j^{(a)}, \Psi^{(i-1)}\big(X_j^{(a)}, Y_j^{(a)}\big)\big)$$

$$= \sum_{k=1}^{Na} a_k^{(i)} \varphi_k\big(X_j^{(a)}, Y_j^{(a)}\big) + \sum_{l=1}^{Nl} b_l^{(i)} p_l\big(X_j^{(a)}, Y_j^{(a)}\big) \quad \text{for } j = 1, 2, \ldots, N_a, \tag{4-13}$$

$$\sum_{k=1}^{Na} a_k^{(i)} p_l\big(X_k^{(a)}, Y_k^{(a)}\big) = 0 \quad \text{for } l = 1, 2, \ldots, N_l. \tag{4-14}$$
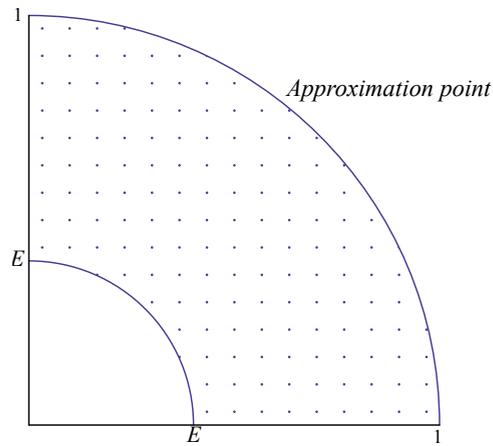

Figure 4. Approximation points.

Once the real coefficients $\{a_k^{(i)}\}_{k=1}^{Na}$ and $\{b_l^{(i)}\}_{l=1}^{Nl}$ are calculated the particular solution of form (4-10) is obtained. In the MFS the approximate homogeneous solution is a linear combination of fundamental solutions:

$$\Psi_h^{(i)}(X,Y) = \sum_{n=1}^{Ns} c_n^{(i)} f s_n(X,Y), \tag{4-15}$$

where $f s_n(X,Y) = f s\big(X,Y,X_n^{(s)},Y_n^{(s)}\big)$ is the fundamental solution defined at the n-th source point. Moreover, $\{X_n^{(s)},Y_n^{(s)}\}_{n=1}^{Ns}$ is a set of source points, placed outside the region considered (the set of source points is presented in Figure 5), and N_s is the number of source points. The coefficients $c_n^{(i)}$ for $n = 1, 2, \ldots, N_s$ are real numbers. These coefficients are to be calculated by solving the linear algebraic equations, which are obtained by introducing (4-8) and (4-15) into the boundary conditions (4-2)–(4-5):

$$\sum_{n=1}^{Ns} c_n^{(i)} f s_n\big(X_m^{(b)}, Y_m^{(b)}\big) = -\Psi_p^{(i)}\big(X_m^{(b)}, Y_m^{(b)}\big) \quad \text{for} \quad \big(X_m^{(b)}, Y_m^{(b)}\big) \in \tilde{\Gamma}_0, \tag{4-16}$$

$$\sum_{n=1}^{Ns} c_n^{(i)} f s_n\big(X_m^{(b)}, Y_m^{(b)}\big) = \Psi_0 - \Psi_p^{(i)}\big(X_m^{(b)}, Y_m^{(b)}\big) \quad \text{for} \quad \big(X_m^{(b)}, Y_m^{(b)}\big) \in \tilde{\Gamma}_{\mathrm{I}}, \tag{4-17}$$

$$\sum_{n=1}^{Ns} c_n^{(i)} \oint_{\tilde{\Gamma}_{\mathrm{I}}} \frac{\partial f s_n(X,Y)}{\partial n} ds = -\oint_{\tilde{\Gamma}_{\mathrm{I}}} \frac{1}{f(X,Y)}(X dY - Y dX) - \oint_{\tilde{\Gamma}_{\mathrm{I}}} \frac{1}{f(X,Y)} d\tilde{u}_z - \oint_{\tilde{\Gamma}_{\mathrm{I}}} \frac{\partial \Psi_p^{(i)}(X,Y)}{\partial n} ds, \tag{4-18}$$

$$\sum_{n=1}^{Ns} c_n^{(i)} \frac{\partial f s_n\big(X_m^{(b)}, Y_m^{(b)}\big)}{\partial n} = -\frac{\partial \Psi_p^{(i)}\big(X_m^{(b)}, Y_m^{(b)}\big)}{\partial n} \quad \text{for} \quad \big(X_m^{(b)}, Y_m^{(b)}\big) \in \tilde{\Gamma}_{\mathrm{S}}, \tag{4-19}$$

where $\{X_m^{(b)}, Y_m^{(b)}\}_{m=1}^{Nb}$ is a set of boundary points (see Figure 5) and N_b is the number of boundary points.
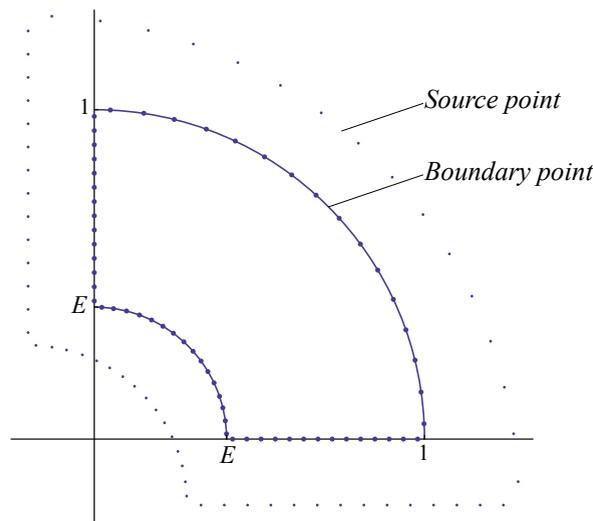

Figure 5. The boundary and source points.

Solution of the system of equations (4-16)–(4-19) introduced to the form of the homogeneous solution (4-15) and to (4-8) gives the approximate solution of the problem. The iteration procedure is stopped if the control parameter defined by the formula

$$d_i = \frac{\sqrt{\sum_{k=1}^{N_t} \left(\Psi^{(i)}(X_k^t, Y_k^t) - \Psi^{(i-1)}(X_k^t, Y_k^t) \right)^2}}{N_t} \quad \text{for} \quad i = 1, 2, \dots \tag{4-20}$$

is a small number. The formula (4-20) is written for N_t trail points (X_k^t, y_k^t) for $k = 1, 2, \dots, N_t$.

5. Numerical experiment

The numerical experiment has been performed to show the accuracy of the proposed algorithm. The MFS has been implemented with the following parameters. The number of approximation points is 100, the number of source points is 40, and the number of boundary points is 30. The distance between the contour of the region under consideration and the contour with the set of source points is chosen as 0.2.

The calculations are performed for the multiquadric RBF given by

$$\varphi\left(X, Y, X_j^{(a)}, Y_j^{(a)}\right) = \sqrt{c^2 + r\left(X, Y, X_j^{(a)}, Y_j^{(a)}\right)}, \tag{5-1}$$

where

$$r\left(X, Y, X_j^{(a)}, Y_j^{(a)}\right) = \sqrt{\left(X - X_j^{(a)}\right)^2 + \left(Y - Y_j^{(a)}\right)^2}.$$

The particular solution for the RBF in the form (5-1) is

$$\phi\left(X, Y, X_j^{(a)}, Y_j^{(a)}\right) = -\frac{1}{3}c^3 \ln\left(c\sqrt{c^2 + r^2\left(X, Y, X_j^{(a)}, Y_j^{(a)}\right)} + c^2\right)$$

$$+ \frac{1}{9}\left(4c^2 + r^2\left(X, Y, X_j^{(a)}, Y_j^{(a)}\right)\right)\sqrt{c^2 + r^2\left(X, Y, X_j^{(a)}, Y_j^{(a)}\right)}. \tag{5-2}$$

The parameter of the chosen RBF (5-1) is $c = 0.1$. The monomials $p_l(X, Y)$ and their corresponding particular integrals $P_l(X, Y)$ are as follows:

l	p_l	P_l	l	p_l	P_l
1	1	$\frac{1}{4}(X^2 + Y^2)$	4	XY	$\frac{1}{12}XY(X^2 + Y^2)$
2	X	$\frac{1}{8}X(X^2 + Y^2)$	5	X^2	$\frac{1}{14}\left(X^4 + X^2y^2 - \frac{1}{6}Y^4\right)$
3	Y	$\frac{1}{8}Y(X^2 + Y^2)$	6	Y^2	$\frac{1}{14}\left(Y^4 + X^2y^2 - \frac{1}{6}X^4\right)$

In the example the torsion of a circular bar (with radius in nondimensional form equal to 1) with a circular centered hollow of radius equal to E is considered. The function related to the shear modulus is defined as

$$\frac{1}{f(X, Y)} = 1 + 5.25\sqrt{X^2 + Y^2}. \tag{5-3}$$

The results for $E = 0.4$ are presented below. The Prandtl function is presented in Figure 6. The unknown value of the Prandtl function on the inner boundary has been calculated. It should have a constant value on the inner boundary. In Table 1 the calculated values of Ψ_0 at some trial points chosen on the inner
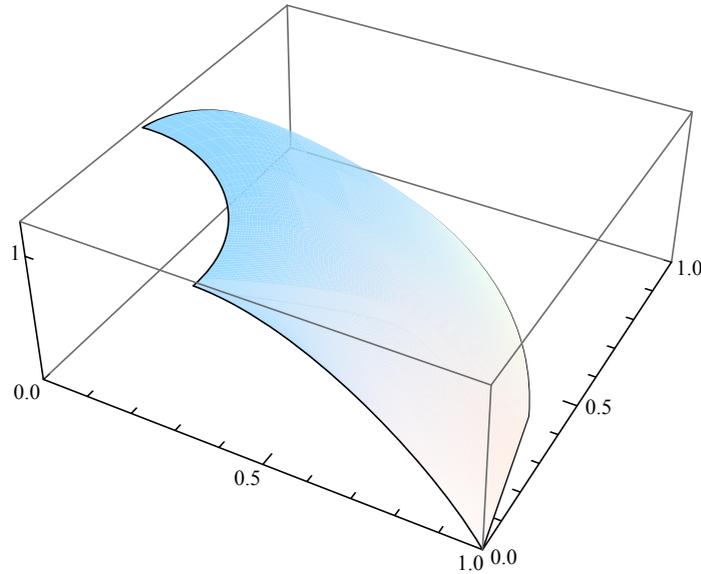
Figure 6. The Prandtl function for a bar with hollow of radius $E = 0.4$.

boundary are presented. The values of Ψ_0 on the boundary are very close to each other. It is correct to take with demanded accuracy Ψ_0 equal to 1.42605.

The accuracy of the obtained result can be confirmed by checking the boundary condition (3-12). The value on the right-hand side of (3-12) is equal to

$$-\oint_{\tilde{\Gamma}_{\mathrm{I}}} \frac{1}{f(X,Y)}(X\,dY - Y\,dX) - \oint_{\tilde{\Gamma}_{\mathrm{I}}} \frac{1}{f(X,Y)}\,d\tilde{u}_z = -0.5026548245743669.$$

X	Y	Ψ_0
0.398766933	0.0313836383	1.426047729150132
0.388947968	0.0933781455	1.426051497720865
0.369551813	0.153073373	1.426050691973953
0.341056066	0.208999426	1.426050690505380
0.3041623862	0.259779219	1.426050814325789
0.2597792193	0.304162386	1.426050908371237
0.208999426	0.341056066	1.426050402589498
0.153073373	0.369551813	1.426051442033329
0.0933781455	0.388947968	1.426049341092722
0.0313836383	0.398766933	1.426054977550235

Table 1. The values of the Prandtl function on the inner boundary for $E = 0.4$.

E	Ψ_0	$\oint_{\Gamma_I}(\partial\Psi/\partial n)\,ds$	$I(E)$
0.1	1.931868393966856	−0.031415926344492	−0.031415926535898
0.2	1.803559095926270	−0.125663706148103	−0.125663706143592
0.3	1.632842169956845	−0.282743338761668	−0.282743338823081
0.4	1.426050772804763	−0.502654824541456	−0.502654824574367
0.5	1.195205510255710	−0.785398163408337	−0.785398163397448
0.6	0.949110141725394	−1.130973355347243	−1.130973355292326
0.7	0.698569048610646	−1.539380400193735	−1.539380400258998

Table 2. The values of the Prandtl function on the inner boundary and checking boundary condition (3-12).

On the other side, the left-hand side of (3-6) is an integral of the normal derivative of the numerically calculated Prandtl function and it equals

$$\oint_{\Gamma_I} \frac{\partial\Psi}{\partial n}\,ds = -0.5026548245414568.$$

It is easy to observe that the difference between both values is 3.29101^{-11}. So, the calculated results are obtained with a very high accuracy.

The problem is solved for a rod with hollow radius $E_i = 0.1i$ for $i = 1, 2, \ldots, 7$. The values of Ψ_0 and the fulfillment of the boundary condition (3-12) are presented in Table 2. It is observed that the difference

$$I(E) = \oint_{\Gamma_I} \frac{\partial\Psi}{\partial n}\,ds - \left(-\oint_{\tilde{\Gamma}_I} \frac{1}{f(X,Y)}(X\,dY - Y\,dX) - \oint_{\tilde{\Gamma}_I} \frac{1}{f(X,Y)}\,d\tilde{u}_z\right)$$

for all cases of E presented in Table 2 are of order 10^{-11} or 10^{-10}. This confirms that the numerical method based on the proposed algorithm is of very high accuracy and gives very good results. It is a suitable tool for solving the problem.

6. Conclusions

In this paper the torsion of a long bone is considered. The long bone is modeled as a bar with circular cross-section with a circular hollow. The proper assumption about the material of the bone have been made. The bone material is treated as a functionally graded material. This paper implements the method of fundamental solutions to solve the problem of long-bone torsion modeled by a boundary value problem with a linear partial differential equation with variable coefficients and boundary conditions. The results of the numerical experiment show that the proposed method gives results with the demanded accuracy. The presented algorithm is a self-validating one. It is possible to prove the high precision of the obtained numerical results by checking the fulfillment of the boundary conditions. The analysis of the numerical results shown in Section 5 confirms that the numerical method based on the proposed algorithm is of very high accuracy and gives very good results. It is a suitable tool to solve the problem.

References

[Arghavan and Hematiyan 2009] S. Arghavan and M. R. Hematiyan, "Torsion of functionally graded hollow tubes", *Eur. J. Mech. A Solids* **28**:3 (2009), 551–559.

[Chen 1964] Y. Chen, "Torsion of nonhomogeneous bars", *J. Franklin Inst.* **277**:1 (1964), 50–54.

[Daegling 2002] D. J. Daegling, "Estimation of torsional rigidity in primate long bones", *J. Hum. Evol.* **43**:2 (2002), 229–239.

[Ecsedi 2009] I. Ecsedi, "Some analytical solutions for Saint-Venant torsion of non-homogeneous cylindrical bars", *Eur. J. Mech. A Solids* **28**:5 (2009), 985–990.

[Elias et al. 2000] J. J. Elias, F. J. Frassica, and E. Y. S. Chao, "The open section effect in a long bone with a longitudinal defect: a theoretical modeling study", *J. Biomech.* **33**:11 (2000), 1517–1522.

[Ely and Zienkiewicz 1960] J. F. Ely and O. C. Zienkiewicz, "Torsion of compound bars: a relaxation solution", *Int. J. Mech. Sci.* **1**:4 (1960), 356–365.

[Fairweather and Karageorghis 1998] G. Fairweather and A. Karageorghis, "The method of fundamental solutions for elliptic boundary value problems", *Adv. Comput. Math.* **9**:1-2 (1998), 69–95.

[Golberg and Chen 1999] M. A. Golberg and C. S. Chen, "The method of fundamental solutions for potential, Helmholtz and diffusion problems", pp. 103–176 in *Boundary integral methods: numerical and mathematical aspects*, edited by M. A. Golberg, Comput. Eng. **1**, WIT Press, Boston, 1999.

[Horgan and Chan 1999] C. O. Horgan and A. M. Chan, "Torsion of functionally graded isotropic linearly elastic bars", *J. Elasticity* **52**:2 (1999), 181–199.

[Kupradze and Aleksidze 1964] V. D. Kupradze and M. A. Aleksidze, "The method of functional equations for the approximate solution of certain boundary value problems", *Ž. Vyčisl. Mat. i Mat. Fiz.* **4**:4 (1964), 683–715. In Russian; translated in *USSR Comput. Math. Math. Phys.* **4**:4 (1964), 82–126.

[Mathon and Johnston 1977] R. Mathon and R. L. Johnston, "The approximate solution of elliptic boundary-value problems by fundamental solutions", *SIAM J. Numer. Anal.* **14**:4 (1977), 638–650.

[Pierce et al. 2004] M. C. Pierce, G. E. Bertocci, E. Vogeley, and M. S. Moreland, "Evaluating long bone fractures in children: a biomechanical approach with illustrative cases", *Child Abus. Negl.* **28**:5 (2004), 505–524.

[Pompe et al. 2003] W. Pompe, H. Worch, M. Epple, W. Friess, M. Gelinsky, P. Greil, U. Hempel, D. Scharnweber, and K. Schulte, "Functionally graded materials for biomedical applications", *Mater. Sci. Eng. A* **362**:1–2 (2003), 40–60.

ANITA USCILOWSKA: anita.uscilowska@put.poznan.pl
Institute of Applied Mechanics, Poznan University of Technology, ul. Jana Pawla II 24, 60-965 Poznan, Poland

AGNIESZKA FRASKA: agnieszka.fraska@put.poznan.pl
Institute of Applied Mechanics, Poznan University of Technology, ul. Jana Pawla II 24, 60-965 Poznan, Poland

JOURNAL OF MECHANICS OF MATERIALS AND STRUCTURES

jomms.net

Founded by Charles R. Steele and Marie-Louise Steele

Cover design: Alex Scorpan

Special issue
Trends in Continuum Physics (TRECOP 2010)